Chemodynamics of soft nanoparticulate metal complexes : from the local particle/medium interface to a macroscopic sensor surface

Chemodynamics of soft nanoparticulate metal complexes: from the local particle/medium interface to a macroscopic sensor surface

Raewyn M. Town[1,3*], José Paulo Pinheiro[2,3] and Herman P. van Leeuwen[3]

[1] Systemic Physiological and Ecotoxicological Research (SPHERE), Department of Biology, University of Antwerp, Groenenborgerlaan 171, 2020 Antwerp, Belgium

[2] Université de Lorraine, Laboratoire Interdisciplinaire des Environnements Continentaux, UMR 7360 CNRS, 15 avenue du Charmois, 54500 Vandoeuvre-les-Nancy, France

[3] Physical Chemistry and Soft Matter, Wageningen University & Research, Stippeneng 4, 6708 WE Wageningen, The Netherlands

Abstract

The lability of a complex species between a metal ion M and a binding site S, MS, is conventionally defined with respect to an ongoing process at a reactive interface, e.g. the conversion and/or accumulation of the free metal ion M by a sensor. In the case of soft charged multi-site nanoparticulate complexes, the chemodynamic features that are operative within the micro environment of the particle body generally differ substantially from those for dissolved similar single-site complexes in the same medium. Here we develop a conceptual framework for the chemodynamics and the ensuing lability of soft (3D) nanoparticulate metal complexes. The approach considers the dynamic features of MS at the intraparticulate level and their impact on the overall reactivity of free metal ions at the surface of a macroscopic sensing interface. Chemodynamics at the intraparticulate level is shown to involve a local reaction layer at the particle/medium interface, whilst at the macroscopic sensor level an operational reaction layer is invoked. Under a certain window of conditions, volume exclusion of the NP body near the medium/sensor interface is substantial and affects the properties of the reaction layer and the overall lability of the nanoparticulate MS complex towards the reactive surface.

Introduction

Nanoparticles (NPs) are defined as entities with at least one external dimension in the range of 1 to 100 nm.[1] Many different types of NPs are present in environmental and biological systems, including those of natural origin, e.g. humic substances and proteins, as well as a range of engineered NPs, e.g. TiO_2, Ag, and nanoplastics. The nature of such NPs encompasses hard (impermeable), core-shell, and soft (permeable) ones. Furthermore, the various NPs may contain a range of reactive sites, S, in terms of both their chemical functionality and electric charge. Accordingly, NPs may serve as complexants for various inorganic and organic ions and molecules, thus modifying the physicochemical speciation of both the associated compounds and the NPs themselves. Nanoparticulate complexants display unique features as a result of the spatial confinement of the reactive sites to the particle body (3D soft case) or the particle surface (2D hard case).[2-5] NPs in aqueous dispersions generally carry a net charge and thus the particles feature an electric potential that is different from that in the surrounding medium.[6-9] The predominant effect of such a particulate electric field is to increase the local concentrations of oppositely charged entities. Accordingly, well charged NPs may exhibit ionic reaction rates that are orders of magnitude greater than their molecular counterparts.[2] This feature can be exploited for smart design of NPs with optimized reactivity, e.g. for catalysis[10] or drug delivery.[11] Obviously, such applications rest on detailed knowledge of the rates of uptake and/or release of ions and/or small molecules by the NPs, e.g. in the context of their response to reactive macrosurfaces. In this regard, nanoparticulate complexants have been observed to exhibit chemodynamic behaviour that is distinct from that of their simple molecular counterparts.[12-14] It is therefore fundamental to establish appropriate means to probe and quantitatively interpret the reactivity of NP species in such settings. In this context, techniques for dynamic speciation analysis are essential tools since they provide information on the fluxes and reactivities of species.[15] The magnitude of the flux of some target free metal ion is generally related to the lability of its complex species, i.e. the extent to which complexes dissociate to release free species on the timescale of their diffusion towards the sensor surface. Available techniques for probing the lability of complex species include various electrochemical methods,[16-19] as well as dynamic forms of techniques such as diffusive gradients in thin film (DGT),[20-

[22] Donnan membrane partitioning (DMT),[23,24] permeation liquid membranes,[25-27] ion-exchange,[28-30] and dynamic solid phase microextraction (SPME)[31-34] for organics.

The concept of lability is well established for the case of molecular complex species for which the dimensions of the complexing ligand are smaller than the non-equilibrium reaction layer, with thickness λ, that extends over the sensing interface.[15,35] Here we consider the most common case in which the uncomplexed target metal ion, M, is the sensed species. Two limiting cases are identified, namely (i) a purely diffusion-limited flux in which the M + S $\leftrightarrow$ MS complexation equilibrium is maintained at any relevant scale so that there is coupled diffusion of the free and complex species of the target ion, and (ii) a kinetically controlled flux that is governed by the rate of dissociation of the complex. For molecular complexes, the approximative Koutecký-Koryta (KK) scheme,[36-39] has shown great utility in describing a wide range of lability issues.[39-42] The KK approximation divides the concentration profiles of free and complexed M in the diffusion layer into a labile and a nonlabile region, separated by the boundary of the reaction layer, i.e. at a distance λ from the macroscopic interface.

The reaction layer concept is based on the rate of re-association of a free ion with a site S and therefore only has physical meaning in the presence of complexing sites. Accordingly for the case of nanoparticulate complexing agents, in which the reactive sites are confined to the particle body, the true reaction layer is bound to be an *intraparticulate* feature.[43] A quantitative description of the lability of nanoparticulate complexes towards a reactive macrosurface thus calls for a more differentiated approach that considers the role of the chemodynamics inside the NP body,[43] in conjunction with the particle/medium exchange of the reactive target species.[44] In the light of recent theoretical insights, we here develop an approach to couple the local particulate processes of association/dissociation and diffusion to/from the particle body with macroscopic fluxes at sensor/medium interfaces.

THEORY

For convenience, unless otherwise stated, the expressions below refer to nanoparticulate complexants in the high charge density regime under conditions such that $\kappa_p r_p > 1$, where r_p is the particle radius and κ_p^{-1} is the intraparticulate Debye screening length.[45,46]

Chemodynamics of metal-NP interactions

The overall process of metal ion binding by NP complexants may often be described in terms of an elaborated Eigen mechanism.[3,47] Analogous with the original formulation for aqueous metal ion complexation by simple molecular ligands,[48] the mechanism for complex formation with NPs distinguishes several steps. As evident from the scheme in Fig. 1, the association process involves the consecutive steps of diffusion of ions to the particle body followed by inner-sphere complex formation, whilst dissociation involves stepwise inner-sphere complex dissociation followed by release of ions from the particle body into the bulk surrounding medium. Diffusion inside particles with a substantial water content is usually faster than extraparticulate diffusion in the aqueous medium.[49]

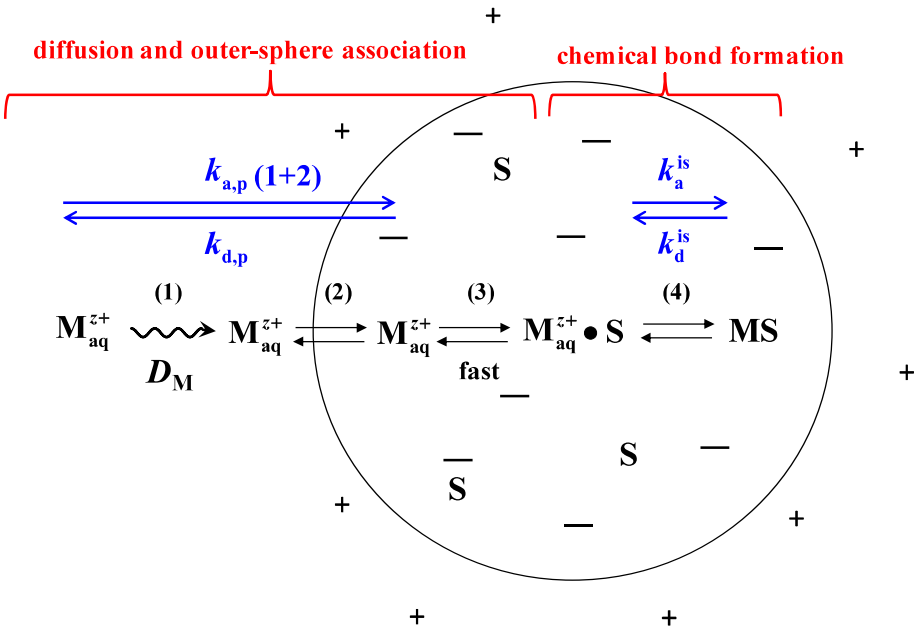

Fig. 1. Steps involved in the associative and dissociative interaction of an aqueous charged metal ion, M_{aq}^{z+}, (z is the charge number) with a spherical soft nanoparticle containing charged or uncharged reactive sites (S) and charged indifferent sites (**–**). The +'s denote the extraparticulate part of the counterionic atmosphere, and the k's represent the pertaining rate constants. The associative steps are (1) diffusion of M_{aq}^{z+} from the bulk solution to the surface of the nanoparticle, (2) incorporation within the particle body as a free hydrated ion, (3) outer-sphere association of M_{aq}^{z+} with S, to form M_{aq}^{z+}•S, and (4) formation of a covalent chemical bond, MS, which generally includes the release of water from the inner hydration layer by M_{aq}^{z+}.

In the high charge density regime, with a charged site separation distance, ℓ_S, of order 1 nm, the outer-sphere volume around a complexing site and the remaining aqueous volume of the particle are at practically the same potential.[50] Accordingly, the intermediate outer-sphere associates M_{aq}^{z+}•S are electrostatically indistinguishable from the intraparticulate free metal ions and interconversion between these species occurs at a timescale of ℓ_S^2/D_M, i.e. on the order of 10^{-9} s. Therefore the outer-sphere formation step generally is not rate-limiting (Fig. 1). Here we consider the situation where ion distributions over the particle body and the medium are electrostatically equilibrated.[3] Rates and rate constants for the complex formation/dissociation reactions will be expressed on a per site basis: for analysis of the chemodynamics inside the NP body the expressions are explicit in terms of the *intraparticulate* conditions, whilst for analysis of the lability towards a macroscopic surface/interface the expressions refer to the average conditions over the entire dispersion.

Complex formation

For the case of diffusive supply of M^{z+} towards a spherical charged NP body, the limiting rate, $R_{a,p}$ can be written as:[3]

$$R_{a,p} = (4\pi N_{Av} r_p D_M \overline{f}_{el,a} / N_S) c_M^* c_S \qquad [\text{mol m}^{-3}\ \text{s}^{-1}] \qquad (1)$$

where D_M is the diffusion coefficient of the free metal ion in the bulk aqueous medium, $\overline{f}_{el,a}$ is the coefficient for conductive diffusion towards the NP,[51] N_S is the number of reactive sites per particle, c_M^* is the concentration of free M in the bulk medium and c_S is the intraparticulate concentration of reactive sites.

The corresponding rate constant is:

$$k_{a,p} = 4\pi N_{Av} r_p D_M \overline{f}_{el,a} / N_S \qquad [m^3\ mol^{-1}\ s^{-1}] \qquad (2)$$

The limiting rate of Eigen type inner-sphere complex formation, R_a^{is}, is given by:[3]

$$R_a^{is} = k_w V^{os} N_{Av} c_M c_S \qquad [mol\ m^{-3}\ s^{-1}] \qquad (3)$$

where V^{os} is the volume around an individual site S that allows for formation of an outer-sphere associate (e.g. ion pair) with M_{aq}^{z+}, and c_M is the intraparticulate concentration of M_{aq}^{z+}. As noted above, in the high charge density limit, the M in an outer-sphere associate M_{aq}^{z+}•S is electrostatically equivalent to the intraparticulate M_{aq}^{z+}.[50] Since c_S corresponds to $N_S / (N_{Av} V_p)$, R_a^{is} can be re-written as

$$R_a^{is} = k_w (N_S V^{os} / V_p)\, c_M \qquad [mol\ m^{-3}\ s^{-1}] \qquad (4)$$

where $(N_S V^{os} / V_p)\, c_M$ corresponds to the concentration of outer-sphere associates, $c_{M•S}$, thus:

$$R_a^{is} = k_w c_{M•S} \qquad [mol\ m^{-3}\ s^{-1}] \qquad (5)$$

The corresponding rate constant follows from eq 3:

$$k_a^{is} = k_w V^{os} N_{Av} \qquad [m^3\ mol^{-1}\ s^{-1}] \qquad (6)$$

The rate constant for the overall association reaction, k_a, can be expressed in a composite form which inherently accounts for intermediate cases in which diffusion to the particle body and inner-sphere complex formation occur on comparable timescales, i.e.:

$$k_a = (1 / k_{a,p} + 1 / k_a^{is})^{-1} \qquad [m^3\ mol^{-1}\ s^{-1}] \qquad (7)$$

Complex dissociation

The limiting rate of diffusion of released M from the spherical particle body into the medium, $R_{d,p}$, is given by:[3]

$$R_{d,p} = \frac{3D_M \overline{f}_{el,d}}{r_p^2 \overline{f}_B} c_M \qquad [\text{mol m}^{-3}\ \text{s}^{-1}] \qquad (8)$$

where $\overline{f}_{el,d}$ is the coefficient for conductive diffusion from the NP surface into the medium. The corresponding diffusion-controlled rate constant, $k_{d,p}$ is given by:

$$k_{d,p} = 3D_M \overline{f}_{el,d}(1 + K_{int} c_S) / r_p^2 \overline{f}_B \qquad [\text{s}^{-1}] \qquad (9)$$

where K_{int} is the intrinsic stability constant of the inner-sphere complex.

The limiting rate of dissociation of inner-sphere complexes, R_d^{is}, is given by:[3]

$$R_d^{is} = \frac{k_a^{is}}{K_{int}} c_{MS} \qquad [\text{mol m}^{-3}\ \text{s}^{-1}] \qquad (10)$$

where k_a^{is} is given by eq 6 and c_{MS} is the intraparticulate concentration of MS. The rate constant for inner-sphere dissociation, k_d^{is}, follows as

$$k_d^{is} = k_a^{is} / K_{int} = k_w V^{os} N_{Av} / K_{int} \qquad [\text{s}^{-1}] \qquad (11)$$

The composite rate constant for the overall dissociation reaction, k_d, which accounts for rate limitation by diffusion from the particle body and by inner-sphere complex dissociation is given by:[52]

$$k_d = (1/k_{d,p} + 1/k_d^{is})^{-1} \qquad [\text{s}^{-1}] \qquad (12)$$

Lability Concepts

We consider processes occurring at a macroscopic reactive interface, e.g. a sensor that converts/accumulates free M after its reactive diffusion from the bulk medium, coupled with release from its NP complex. The setting is shown schematically in Fig. 2. The contributing factors involve (i) the volume complexation reaction i.e. the dynamic nature of the NP complex MS and its ability to maintain equilibrium with the changing concentration of free M in the surrounding medium, as well

as (ii) the relative overall rates of metal complex dissociation and diffusive supply towards the interface.

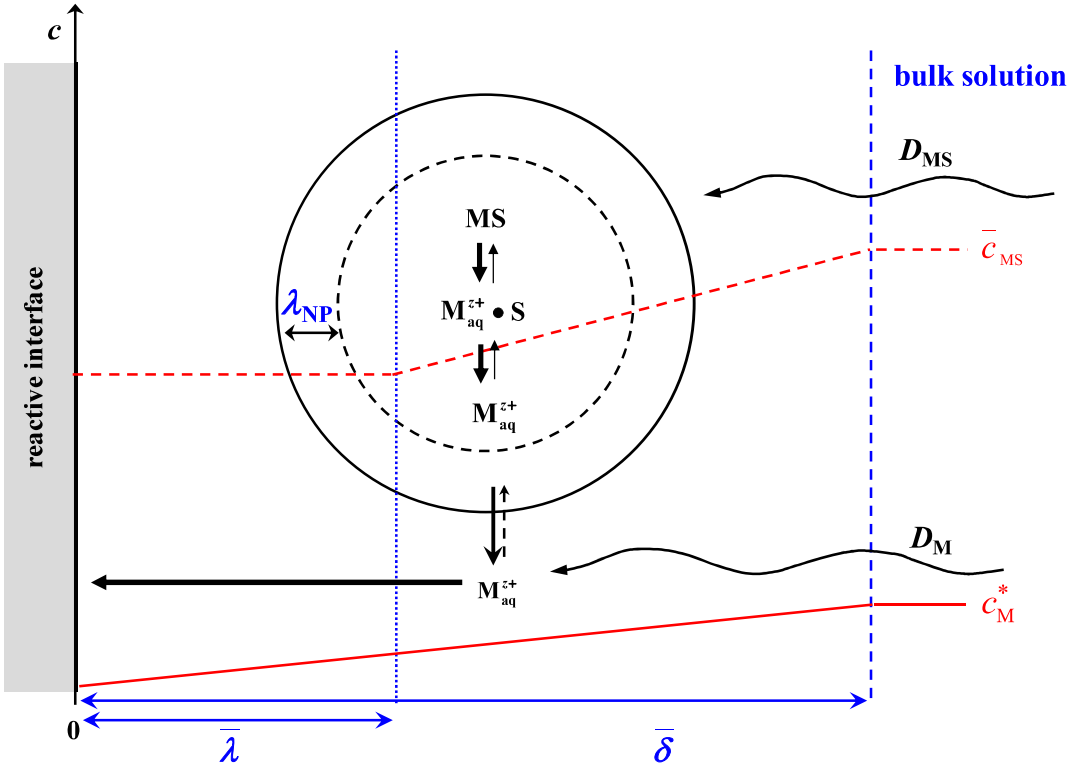

Figure 2. Schematic view of the various processes governing the flux of M towards a macroscopic interface that reacts with free M^{z+}_{aq}, in an aqueous dispersion of nanoparticulate complexes of M. The concentration gradient of the free M^{z+}_{aq} in the medium, c^*_M, is indicated by the solid red line, and the gradient in the average concentration of MS complexes within each spatial zone, $\bar{c}_{MS}$, is indicated by the dashed red line. For clarity, the size of the NP is exaggerated and arbitrary thicknesses are shown for the intraparticulate reaction layer, λ_{NP}, the operational reaction layer at the macroscopic interface, $\bar{\lambda}$, and the mean solution diffusion layer for M^{z+}_{aq} and MS, $\bar{\delta}$.

Intraparticulate chemodynamics

The notion of lability with respect to the releasing particle/medium interface only has conventional meaning in the context of a pertaining reaction layer. Since the release of free M^{z+}_{aq} is the relevant process at the NP/medium interface, a reaction layer should here take the form of an *intraparticulate*

reactive outer shell (Fig. 2).[43] Quantitative description of λ_{NP} is not straightforward because steady-state diffusion does not hold within particle bodies in the nano size range. Instead, rather cumbersome transient conditions govern the release process; a couple of basic non-complex cases for spherical bodies have been drawn to analytical release-time dependencies in Crank.[49] For metal-complexing nanoparticles, the λ_{NP} for rapidly dehydrating metal ions such as Pb^{2+}_{aq} and Cu^{2+}_{aq} with k_w of the order of 10^9 s^{-1},[53-56] will generally be thinner than that for slowly dehydrating metal ions, e.g. Ni^{2+}, with k_w = $3x10^4$ s^{-1}.[53,57-59]

The slow step in the dissociative release of M^{z+}_{aq} at the NP/medium interface may be identified by comparing the relative timescales for dissociation of MS and diffusion of the free M^{z+}_{aq} from the particle body to the bulk medium. Since intraparticulate diffusion is generally fast compared to the extraparticulate diffusion,[49] assessment of the dynamic nature of MS thus reduces to comparing the timescale for extraparticulate diffusion, τ_{diff}:[52]

$$\tau_{diff} = 1 / k_{d,p} \quad (13)$$

with the timescale for inner-sphere complex dissociation *within* the particle body, τ_{diss}:

$$\tau_{diss} = 1 / k_d^{is} = K_{int} / k_a^{is} \quad (14)$$

Accordingly, we may define a dynamic index for nanoparticulate MS, $\mathcal{D}_p$:

$$\mathcal{D}_p = \tau_{diff} / \tau_{diss} \quad (15)$$

such that when $\mathcal{D}_p >> 1$, equilibration of c_{MS} is controlled only by the divergent diffusion from the particle surface at $r = r_p$ into the bulk medium at $r \geq 2r_p$ (see Fig. 3). At the other extreme, where $\mathcal{D}_p << 1$, diffusion is the fast step and then the chemical dissociation of the inner-sphere complex MS is controlling the rate of release of M^{z+}_{aq} from the NP body.

Volume complexation reaction

The chemodynamics of dispersed nanoparticulate complexes is involved with the frequency of exchange of free M_{aq}^{z+} between the *bulk* dispersion medium and MS within the particle body. Accordingly, for description of processes at the macroscopic level, the rate expressions are formulated in terms of concentrations averaged over the entire volume of the dispersion. Since $c_M = \overline{f}_B\, c_M^*$, where $\overline{f}_B$ is the Boltzmann equilibrium partitioning factor, the expression for k_a^{is} becomes:

$$k_a^{is} = k_w V^{os} N_{Av} \overline{f}_B \qquad [m^3\ mol^{-1}\ s^{-1}] \qquad (16)$$

In terms of a conventional volume complexation reaction, the system is dynamic on the timescale of interest, *t*, if

$$k_a \bar{c}_S t, \quad k_d t \quad >> 1 \qquad (17)$$

where the applicable k_a and k_d are the composite rate constants for the overall association and dissociation processes (with k_a^{is} given by eq 16) and $\bar{c}_S$ is the concentration of sites averaged over the dispersion volume. In the context of a bulk volume reaction, a dynamic system implies that there is frequent interchange between free M_{aq}^{z+} in the bulk medium and MS on the timescale of interest. At the other extreme, with $k_a \bar{c}_S t, \quad k_d t \quad << 1$ the system is denoted as inert since it does not significantly re-equilibrate in response to a change in species concentrations in the surrounding aqueous medium.

Lability at a macroscopic reactive interface: Koutecký-Koryta (KK) approximation revisited

For purposes of determining the flux towards a reactive interface, e.g. as relevant for dynamic sensor measurements of free M_{aq}^{z+} in an aqueous dispersion of nanoparticulate MS, it is necessary to compare the rate of release of M_{aq}^{z+} from the NP body with the rate of diffusive supply of MS towards the interface. Within the diffusion layer, the gradient in concentration of M_{aq}^{z+} in the local medium drives release of M_{aq}^{z+} from the particle body (Fig. 2). For macroscopic reactive interfaces, the mean thickness of the diffusion layer for M_{aq}^{z+} and MS, $\overline{\delta}$, is typically of the order of 10^{-4} m,[60] i.e. much greater than the radius of the NP, r_p. This leads to a modest Δc_M between the front and back of an NP:

e.g. for a $\overline{\delta}$ of 100 μm, an NP with a radius of 50 nm feels a gradient of only 0.001 c_M^*. Hence an individual NP experiences essentially the same external concentration of M_{aq}^{z+} over its entire surface. The extent of release of M from the NP body depends on the local concentration of free M_{aq}^{z+} in the medium, $c_{M,medium}$, at the position of the NP complex: dissociation stops when equilibrium is re-established between the NP body and the local $c_{M,medium}$. The nearer an NP comes to the sensor surface, the lower the remaining c_{MS} and hence the lower the rate of release of M_{aq}^{z+}. As a consequence, the re-equilibration becomes incomplete at a certain distance from the surface. If this distance is very small compared to $\overline{\delta}$, the system is effectively labile. This notion is conceptually analogous to implementation of the KK approximation and the ensuing lability criterion developed for molecular ligands.[15]

The KK approximation divides the concentration profiles of free and complexed M in the diffusion layer into a labile and a nonlabile region, separated by the boundary of a reaction layer that extends along the macroscopic interface. The reaction layer concept only has meaning in the presence of reactive sites S. Accordingly, application of the KK approximation to the case of nanoparticulate complexes requires an *operational* reaction layer thickness, $\overline{\lambda}$, to be invoked at the macroscopic interface (Fig. 2). In the NP case, such a reaction layer is not a permanent one because the reactive sites are restricted to the NP body which is moving around. Thus the operational reaction layer should be based on the time-averaged presence of particle body volume which comprises a corresponding time-averaged complexing site concentration. On the basis of this c_S, the reaction layer concept may still have practical utility for estimating the lability of nanoparticulate complexes towards a macroscopic reactive interface.

Following the approach for molecular ligands,[15,52] we derive $\overline{\lambda}$ from the mobility of free M_{aq}^{z+} in the aqueous dispersion, i.e. its diffusion coefficient, D_M, and its mean free lifetime $1/k_a\overline{c_S}^{\lambda}$, as well as the mobility of the complex MS ($\approx D_p$) and its mean free lifetime ($1/k_d$):

$$\bar{\lambda} = \left(\frac{k_a \bar{c}_S^{\lambda}}{D_M} + \frac{k_d}{D_p} \right)^{-1/2} \tag{18}$$

where k_a and k_d are the composite rate constants, with k_a^{is} given by eq 16, and $\bar{c}_S^{\lambda}$ denoting the effective average site concentration within the reaction layer zone. The approach implies that when $\bar{\lambda}$ has the same order of magnitude as the NP body, a *volume exclusion* effect will come into effect. Then the time-averaged volume fraction of the NP that lies within the reaction layer, ϕ_λ, will be less than that in the bulk dispersion, ϕ^*, as shown schematically in Fig. 3.

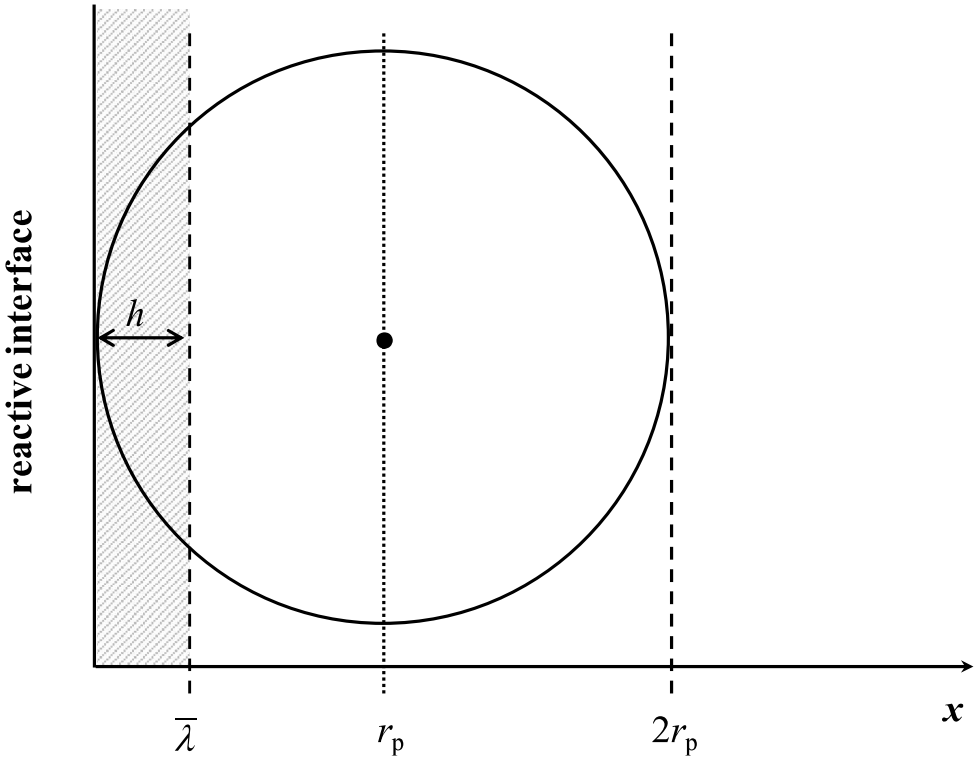

Fig. 3 Schematic representation of a spherical nanoparticle at a macroscopic reactive interface, together with a certain operational reaction layer with thickness $\bar{\lambda}$, highlighted with grey shading. For the case shown, the radius of the particle, r_p, is greater than the thickness of the reaction layer. The solid dot denotes the center of the particle, and h denotes the height of the spherical cap that lies within the reaction layer zone, i.e. $h = \bar{\lambda}$.

In the following, it will be assumed that there is no interaction whatsoever between the NP and the macroscopic surface. This implies that the distribution of NPs over the medium volume is completely random down to a distance r_p from the surface. Within the layer from $x = r_p$ to $x = 0$ there will be a gradual reduction of the NP volume fraction together with similar reduction of the amount of complexing sites S: $\phi_\lambda < \phi^*$. For cases where the NP is much smaller than the reaction layer thickness, we obviously have $\phi_\lambda \approx \phi^*$. When volume exclusion is operative, the proportion of the NP volume that lies within the reaction layer zone must be taken into account in computing the magnitude of the kinetic flux of M_{aq}^{z+} towards the sensor surface. For the supposedly spherical nanoparticles this volume fraction has the shape of a spherical cap with a volume given by:[61]

$$V_{cap} = \pi \bar{\lambda}^2 (3r_p - \bar{\lambda}) / 3 \tag{19}$$

where $\bar{\lambda}$ = the cap height, h (see Fig. 3). For hard 2D NPs with surface complexation, the relevant cap surface area is

$$A_{s,cap} = 2\pi r_p \bar{\lambda} \tag{20}$$

For example, in the particular case of a soft (3D) particle with $\bar{\lambda} = r_p$, the effective NP volume inside the reaction layer corresponds to the average over all positions of the particle center between r_p and $2r_p$, i.e. h from 0 to r_p:

$$\frac{\pi}{3r_p}\int_0^{r_p}(3r_p h^2 - h^3)\mathrm{d}h = \frac{\pi}{4}r_p^3 \tag{21}$$

For the general 3D case, the interpretation requires taking the average over all positions from $x = 0$ to $x = \bar{\lambda}$, i.e. h runs from 0 to r_p:

$$\frac{\pi}{3\bar{\lambda}}\int_0^{\bar{\lambda}}(3r_p h^2 - h^3)\mathrm{d}h = \frac{\pi}{3}\left[r_p \bar{\lambda}^2 - \frac{1}{4}\bar{\lambda}^3\right] \tag{22}$$

Thus, e.g. for the case where $\bar{\lambda}$ = ½ r_p, the time average volume of the NP body that lies within the reaction layer is *ca.* $0.23\, r_p^3$. As a consequence, each NP contributes only a fraction of $0.23/(4\pi/3)$ of its volume and its ligand sites to the reaction layer volume, i.e. some 5%. In terms of the KK

approximation, this implies that the average concentration of S inside the reaction layer would be only 5% of the concentration at $x = \bar{\lambda}$.

For hard (2D) NPs, the proportion of the particle surface area that lies within the reaction layer follows directly from the ratio $\bar{\lambda}/r_p$, i.e.:

$$A_{cap} = 2(\bar{\lambda}/r_p)\pi r_p^2 \quad (23)$$

As a consequence, each NP contributes the fraction of $(\bar{\lambda}/r_p)/2$ of its surface area and ligand sites to the reaction layer volume. For a given r_p and $\bar{\lambda}$, the extent to which the surface area of hard 2D particles is excluded from the reaction layer is significantly less than the extent of volume exclusion experienced by soft 3D particles. For example, for the case of $\bar{\lambda} = ½\ r_p$, a 2D particle has 25% of its surface available for dissociation of MS within the reaction layer, whilst a 3D particle contributes 5% of its volume.

The lability parameter for nanoparticulate MS, $\mathcal{L}_{NP}$, may now be defined in the same general manner as for molecular ligands, i.e. as the ratio of the kinetic and diffusive fluxes. The kinetic flux J_{kin}, represents the rate at which M_{aq}^{z+} is released from the particle body. Since the diffusion-controlled release of M_{aq}^{z+} by the NP can be considered to be fast compared to the macrodiffusion process, all cases with the dynamic index $\mathcal{D}_p >> 1$ (eq 15) lead to fully diffusion-controlled labile behaviour. Consequently, only the case of release controlled by the rate of chemical dissociation of MS is relevant for considering J_{kin}, that is:

$$J_{kin} = k_d^{is} \bar{c}_{MS}^{\lambda} \bar{\lambda} \quad (24)$$

where $\bar{c}_{MS}^{\lambda}$ is the average concentration of MS within the macroscopic reaction layer zone, i.e. taking into account the volume exclusion effects described above.

The diffusive flux, J_{dif}^{*}, represents the rate at which *all forms* of M present in the dispersion arrive at the macroscopic interface. These include the free $\mathrm{M}_{\mathrm{aq}}^{z+}$ in the bulk dispersion, as well as the various intraparticulate forms, i.e. the free $\mathrm{M}_{\mathrm{aq}}^{z+}$, the inner-sphere complex MS, and any other relevant species, e.g. electrically condensed M ions.[62-64] Since the diffusion takes place on a macroscopic scale, the various concentrations now should be expressed in terms of their average values over the whole dispersion volume. The ensuing expression for J_{dif}^{*} is given by:

$$J_{\mathrm{dif}}^{*} = \overline{D}(c_{\mathrm{M}}^{*} + \bar{c}_{\mathrm{MS}} + \bar{c}_{\mathrm{M}} + ...) / (1/\overline{\delta} + 1/r_0)^{-1} \tag{25}$$

where the overbar on the concentration terms denotes the intraparticulate forms of M expressed as smeared-out averages over the dispersion, r_0 is the radius of the sensing surface and $\overline{\delta}$ is the mean diffusion layer thickness as determined by $\overline{D}$, the mean diffusion coefficient for the complex system:

$$\overline{D} = \frac{D_{\mathrm{M}} c_{\mathrm{M}}^{*} + D_{\mathrm{p}}(\bar{c}_{\mathrm{MS}} + \bar{c}_{\mathrm{M}} + ...)}{c_{\mathrm{M,t}}} \tag{26}$$

where $c_{\mathrm{M,t}}$ is the total metal concentration in the entire dispersion. Note that eq 26 implies that all of the intraparticulate free $\mathrm{M}_{\mathrm{aq}}^{z+}$ diffuses with mobility D_{p}.

The lability index, $\mathcal{L}_{\mathrm{NP}}$, follows as:

$$\mathcal{L}_{\mathrm{NP}} = J_{\mathrm{kin}} / J_{\mathrm{dif}}^{*} = k_{\mathrm{d}}^{\mathrm{is}} \bar{c}_{\mathrm{MS}}^{\lambda} \overline{\lambda} / \left(\overline{D}(c_{\mathrm{M}}^{*} + \bar{c}_{\mathrm{MS}} + \bar{c}_{\mathrm{M}} + ...) / (1/\overline{\delta} + 1/r_0)^{-1} \right) \tag{27}$$

For $\mathcal{L}_{\mathrm{NP}} >> 1$, the system is labile with respect to the macroscopic interfacial reaction, and the flux of M from the NP body towards the reactive interface is the diffusion controlled one, J_{dif}^{*}. At the other limit where $\mathcal{L}_{\mathrm{NP}} << 1$, the system is nonlabile and the flux of $\mathrm{M}_{\mathrm{aq}}^{z+}$ from the NP body towards the reactive interface is the kinetically controlled one. Taking together all of the preceding considerations, a chemodynamic scheme for nanoparticulate metal complexes can be constructed (Fig. 4).

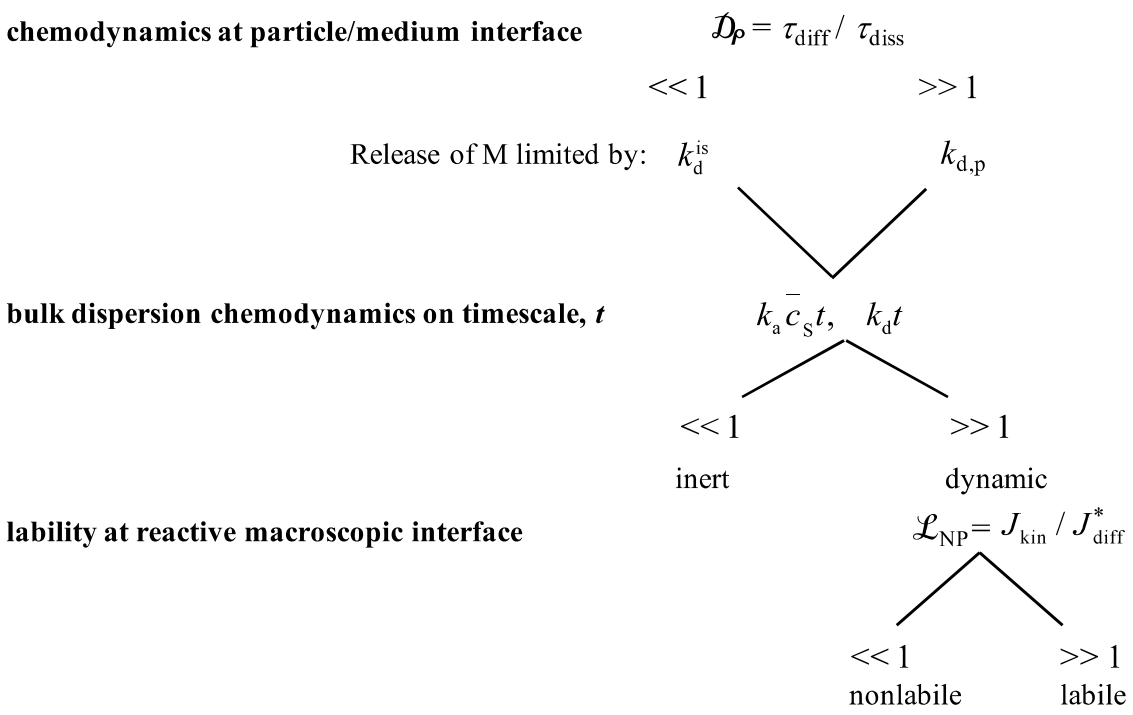

Fig. 4. Scheme for defining the chemodynamic behavior of nanoparticulate metal complexes.

RESULTS AND DISCUSSION

The theoretical framework may serve to explore the effects of basic features of M_{aq}^{z+} (k_w), MS (K_{int}) and the NP (r_p) on the nature of the rate-limiting steps in the associative and dissociative processes and the ensuing chemodynamic features of the MS complexes at the intraparticulate and macrointerfacial levels. All computations refer to the high charge-density case for a given intraparticulate concentration of reactive sites, c_S.

Rate-limiting step in the overall associative process

The rate constant for the overall association process, k_a, eq 7, is independent of the magnitude of the intrinsic binding constant, K_{int}. The rate-limiting step for association is determined by the relative magnitude of the rate of diffusive supply of M_{aq}^{z+} towards the NP body (eq 1) and the rate of inner-sphere complex formation *within* the particle (eq 3). Figure 5 compares k_a with k_a^{is} for a range of 3D particle sizes and metal dehydration rate constants. For all r_p considered, inner-sphere complex formation is rate-limiting for k_w values less than *ca.* 10^5 s^{-1}. As k_w increases, the association rate is

increasingly limited by diffusion towards the particle surface and thus $k_{a,p}$ progressively becomes the predominant contributor to k_a. The plateau regions in Figure 5 are attained when k_a approaches $k_{a,p}$ and the association process has become essentially independent of k_w. The larger r_p, the lower the k_w value at which $k_a \approx k_{a,p}$, in line with previous findings.[50]

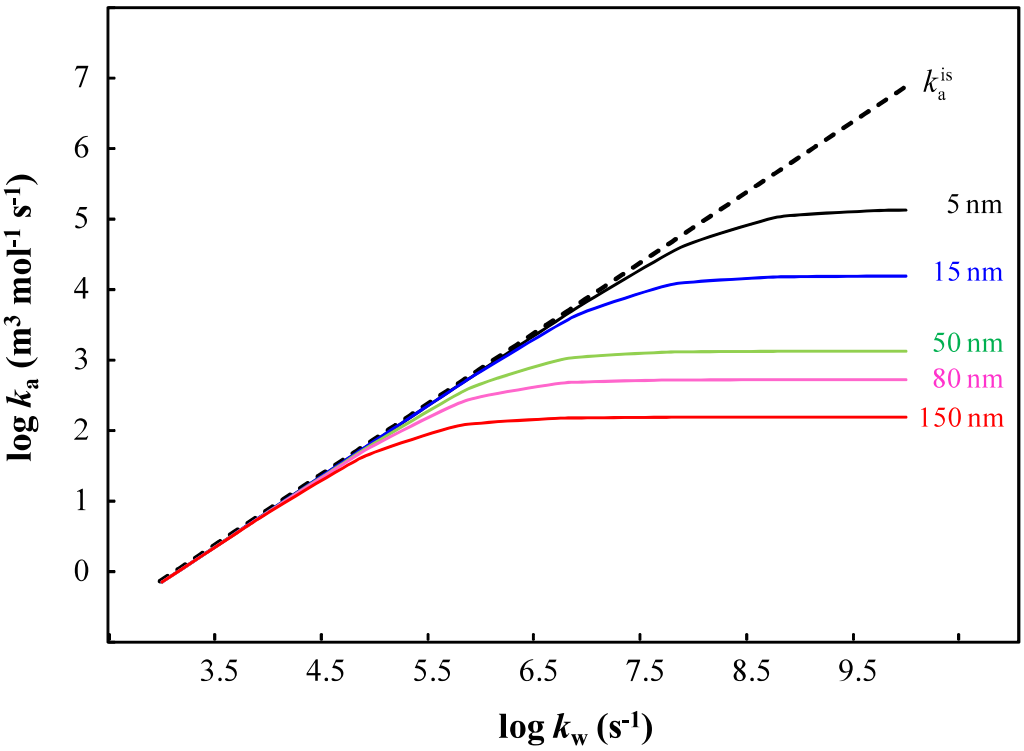

Figure 5. Comparison of the rate constant for inner-sphere complex formation, k_a^{is} (eq 6, dashed black line) with the overall association rate constant, k_a (eq 7, solid curves), for a range of 3D particle radii as a function of the metal dehydration rate constant, k_w. The various r_p values are indicated on the figure. Computations are performed for: c_S = 700 mol m^{-3}, D_M = 8x10^{-10} m^2 s^{-1}.[65]

Rate-limiting step in the overall dissociative process

In addition to the effect of the parameters r_p and k_w, the overall rate of dissociation is also influenced by the magnitude of K_{int} via its impact on both $k_{d,p}$ (eq 9) and k_d^{is} (eq 11). Figure 6 compares the values of the composite k_d (eq 12) and k_d^{is} for a range of 3D particle radii as a function of the metal dehydration rate constant, k_w, for a K_{int} value of 10 m^3 mol^{-1}. As k_w increases, the dissociation rate becomes increasingly limited by diffusion from the particle surface to the bulk medium and thus $k_{d,p}$

progressively becomes the predominant contributor to k_d. For the arbitrarily chosen K_{int} value of 10 m^3 mol^{-1}, k_d^{is} is rate limiting over almost the entire range of r_p and k_w values considered herein, with $k_{d,p}$ only becoming significant for r_p greater than *ca.* 50 nm at high k_w (Fig. 6).

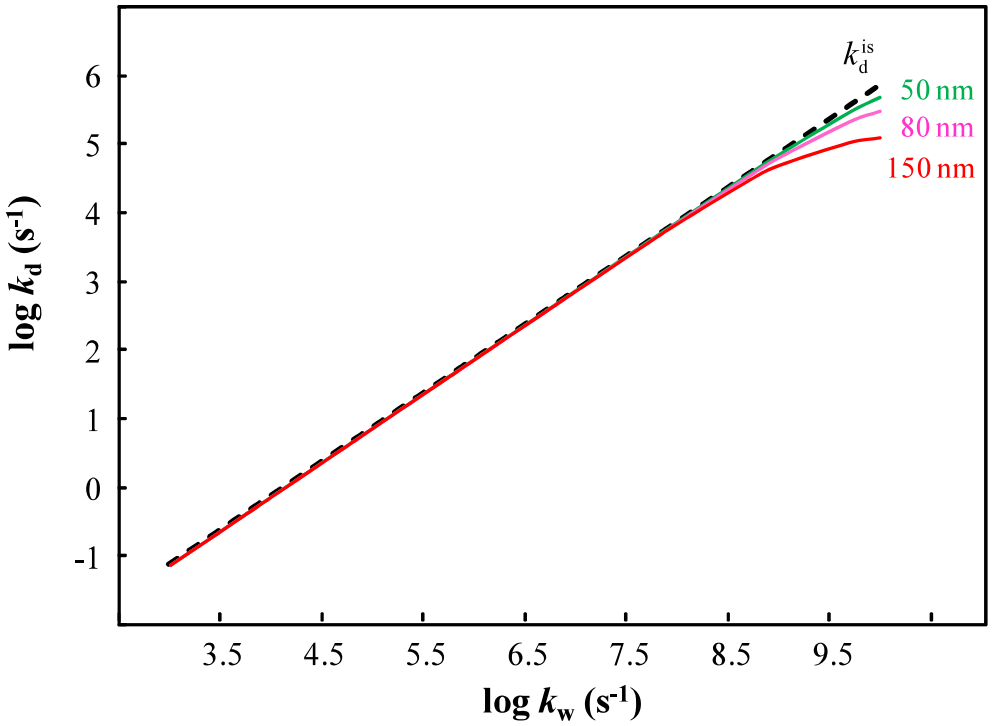

Figure 6. Comparison of the rate constant for dissociation of the inner-sphere complex, k_d^{is} (eq 11, dashed black line) with the overall dissociation rate constant, k_d (eq 12, solid curves), for a range of 3D particle radii as a function of the metal dehydration rate constant, k_w. For r_p values of 5 and 15 nm, k_d is practically equal to k_d^{is} over the entire k_w range shown. Computations are performed for: K_{int} = 10 m^3 mol^{-1}; c_S = 700 mol m^{-3}, D_M = 8x10^{-10} m^2 s^{-1}.[65]

Operational reaction layer thickness at a macroscopic interface

A starting value for $\bar{\lambda}$ is computed via eq 18 using the average site concentration in the dispersion, $\bar{c}_S$. The ensuing volume fraction of the NP body that lies within $\bar{\lambda}$, ϕ_λ, is then computed for the given r_p and the applicable 3D or 2D geometry (eq 22 or eq 23, respectively). The value for ϕ_λ allows for an estimate of the effective concentration of reactive sites, $\phi_\lambda \bar{c}_S$, within the reaction layer. For the conditions considered herein, when volume exclusion becomes relevant, $\bar{\lambda}$ is insensitive to $\bar{c}_S^{\lambda}$

because the dissociative term has become the predominant factor in $\bar{\lambda}$ (eq 18). Accordingly, a single iteration step suffices to obtain ϕ_λ, which then only influences the effective concentration of the dissociating MS in the macroscopic reaction layer, $\bar{c}^{\lambda}_{\mathrm{MS}} = \phi_\lambda \bar{c}_{\mathrm{MS}}$.

Lability of nanoparticulate MS at a reactive interface

The lability index, $\mathcal{L}_{\mathrm{NP}}$, for nanoparticulate complexes MS at a macroscopic interface, reactive towards $\mathrm{M}^{z+}_{\mathrm{aq}}$, is computed via eq 27, together with the composite rate constants, k_{a} and k_{d} and the operational reaction layer thickness, $\bar{\lambda}$. Since the lability towards a sensing surface is related to the free $\mathrm{M}^{z+}_{\mathrm{aq}}$ in the bulk dispersion medium, $k^{\mathrm{is}}_{\mathrm{a}}$ is given by eq 16. Computations were performed for a K_{int} of 10^3 $\mathrm{m^3\ mol^{-1}}$ and a sensor radius of 10^{-6} m, e.g. a microelectrode. These conditions were chosen so that for each r_{p} the lability transitions from nonlabile to labile over the range of k_{w} values considered. As the radius of the sensing surface is increased, the window of particle radii over which the effect of volume exclusion from the macroscopic reaction layer is operative shifts to larger r_{p}. For all conditions, $\mathcal{D}_p$ is much less than unity, i.e. the overall rate of release of $\mathrm{M}^{z+}_{\mathrm{aq}}$ by the particle is limited by inner-sphere dissociation (eq 15). The results are shown in Figure 7. Over most of the k_{w} range considered, lability increases with increasing k_{w}, whilst for a given k_{w} lability increases with increasing r_{p}. However, deviations from these trends are observed as the macroscopic reaction layer becomes thinner and volume exclusion of the NP body comes into effect.

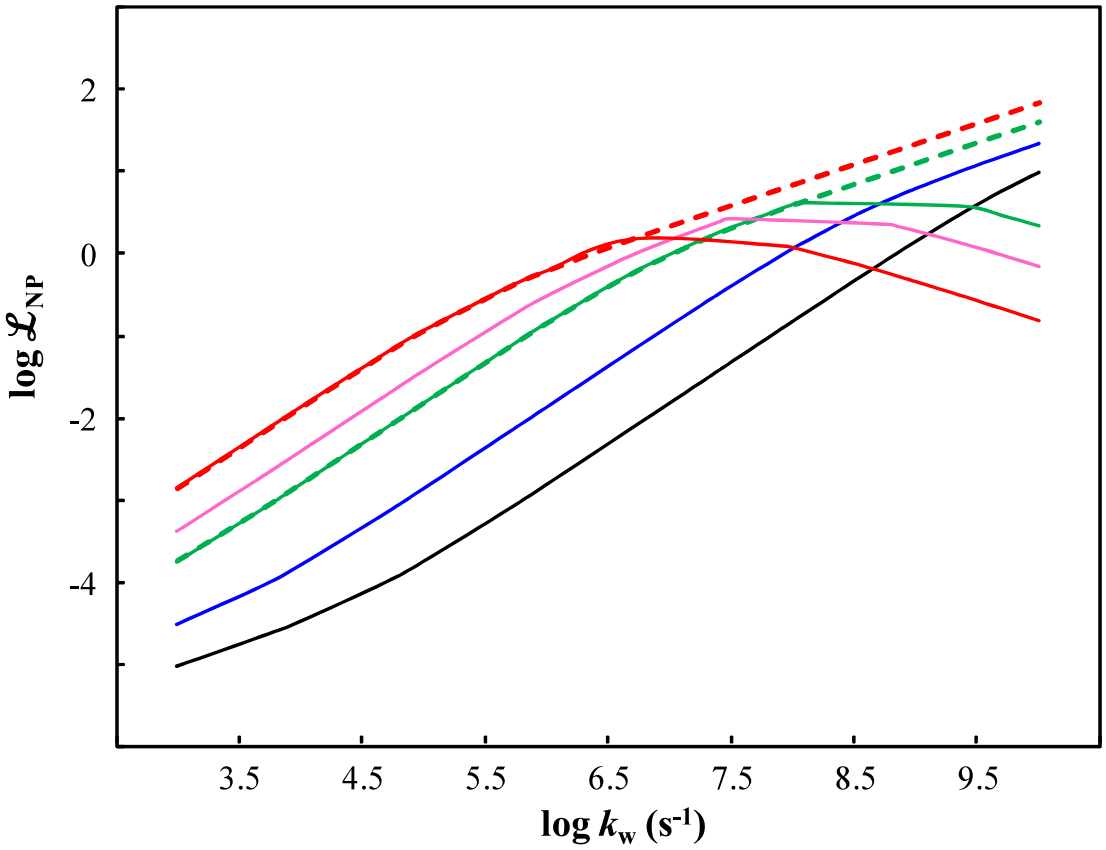

Figure 7. Lability index, $\mathcal{L}_{NP}$, for nanoparticulate metal complexes towards a reactive surface according to eq 27, as a function of the metal ion's dehydration rate constant, k_w. The solid curves are computed by taking account of volume exclusion effects in the macroscopic reaction layer zone for particle radii, r_p, of 5 nm (black), 15 nm (blue), 50 nm (green), 80 nm (pink), and 150 nm (red). Also shown are the $\mathcal{L}_{NP}$ values obtained if volume exclusion is ignored for r_p of 50 nm (green dashed curve) and 150 nm (red dashed curve). Computations are performed for $K_{int} = 10^3$ m^3 mol^{-1}, $\bar{c}_S = 0.7$ mol m^{-3} (i.e. volume fraction in the dispersion equal to 10^{-3} *cf.* Figs. 5 and 6), $\bar{c}_{MS} = 0.03$ mol m^{-3}, $D_M = 8\text{x}10^{-10}$ m^2 s^{-1},[65] D_p computed using the Stokes-Einstein equation,[66] $r_0 = 10^{-6}$ m.

The significance of accounting for volume exclusion effects in defining the operational reaction layer thickness is shown in Fig. 7. The dashed lines for r_p values of 50 and 150 nm correspond to the erroneously high value of $\mathcal{L}_{NP}$ that is obtained if volume exclusion is ignored, i.e. the kinetic flux is overestimated if it is assumed that the average concentration of MS within the macroscopic reaction

layer zone is the same as that in the bulk dispersion. When volume exclusion is taken into account, a decrease in lability is observed at high k_w values. This feature reflects the progressive reduction in the concentration of MS in the reaction layer zone as a consequence of the decreasing thickness of this layer. Note that this effect leads to an inversion of the lability order at high k_w, i.e. the NP with the largest r_p is the least labile, in contrast with the conventional impact of the size of the complex species on lability.[15] The impact of volume exclusion in the reaction layer on the macroscopic lability of nanoparticulate MS increases with increasing r_p and is more dramatic for 3D particles than for 2D ones (eq 22 *cf*. eq 23). The results shown in Fig. 7 for a K_{int} of 10^3 m^3 mol^{-1} correspond to a window of conditions in which exclusion of the NP body from the macroscopic reaction layer zone is significant: as K_{int} decreases, the system becomes more labile and thus the effect becomes immaterial, whilst as K_{int} increases, the effect decreases because the macroscopic reaction layer thickness increases due to the dominance of the dissociative term in eq 18. These features lead to a dampening in the link between K_{int} and $\mathcal{L}_{NP}$. Accordingly, comparison of dynamic chemical speciation information for 3D particles such as humic acids[62] with that for 2D particles such as silica[11] requires rigorous accounting for all the involved factors.

In addition, the effect of volume exclusion will decrease as the solution diffusion layer thickness increases. That is, upon changing the sensor from a microelectrode (r_p of the order of 10^{-6} m) to a conventional electrode ($\overline{\delta}$ of the order of 10^{-4} m[60]), to a DGT device ($\overline{\delta} \approx 1$ mm[67]), a given MS complex becomes increasingly labile (classical behavior)[15,68-70] and thus the significance of volume exclusion effects decreases. In this context it is relevant to note that large particles containing electroactive components have been observed to generate current peaks upon contact with an electrode surface,[71,72] i.e. discharge upon contact takes over from discharge via the medium. Such discharge upon contact would offer a potential escape from volume exclusion effects for larger particles. Measurement of the lability of nanoparticulate metal complexes by a suite of dynamic sensors would provide a practical means to estimate the extent of volume exclusion.

Conclusions and outlook

The chemodynamics of nanoparticulate complexes have been considered at the local intraparticulate level as well as at the level of lability towards a macroscopic sensor. *Intraparticulate* lability is an intrinsic property of the NP, governed by the relative rates of dissociation of inner-sphere complexes and diffusion of free M_{aq}^{z+} within the individual nanoparticle. In the local microenvironment of the NP body, an intraparticulate reaction layer may be developed at the particle/medium interface: when the thickness of this non-equilibrium shell is much less than the particle radius, then MS is labile towards release of M_{aq}^{z+} at the particle/medium interface. At the macroscopic level, the lability of nanoparticulate MS is governed by the relative rates of *release* of M_{aq}^{z+} from the particle body and the diffusive supply of all forms of M to the reactive interface. The stereometrically unavoidable phenomenon of partial exclusion of the NP body fraction from the reaction layer at the sensor/medium interface was found to be operative within a certain window of conditions. In general, the relevance of the NP volume exclusion effect increases with increasing particle radius (r_p) and increasing dehydration rate constant (k_w) of the metal ion M, while moderating the link between the stability of MS and its macroscopic lability. Accordingly, proper identification of exclusion effects in the macroscopic reaction layer is fundamental to rigorous interpretation of fluxes for nanoparticulate complexes as measured by conventional dynamic metal speciation sensors, as well as for any type of comparison between the chemodynamic behavior of different types of nanoparticles.

Symbols and Abbreviations

MS	inner-sphere complex with a nanoparticulate reactive site
NP	nanoparticle
S	reactive site that covalently binds a metal ion
c_M^*	bulk concentration of free metal ion M_{aq}^{z+} (mol m^{-3})
c_M	intraparticulate concentration of free M_{aq}^{z+} (mol m^{-3})
$c_{M\bullet S}$	intraparticulate concentration of outer-sphere complexes (mol m^{-3})

c_{MS}	intraparticulate concentration of inner-sphere complexes (mol m^{-3})
$\bar{c}_{MS}$	average concentration of inner-sphere complexes in the whole dispersion (mol m^{-3})
$c_{M,t}$	total metal concentration in the whole dispersion (mol m^{-3})
$\bar{c}_S$	average concentration of reactive sites in the whole dispersion (mol m^{-3})
$\bar{c}_S^{\lambda}$	average concentration of reactive sites in the operational reaction layer zone at a macroscopic interface (mol m^{-3})
c_S	intraparticulate concentration of binding sites (mol m^{-3})
$\bar{\delta}$	mean diffusion layer thickness for M_{aq}^{z+} and MS (m)
D_M	diffusion coefficient of the metal ion M_{aq}^{z+} in aqueous solution (m^2 s^{-1})
$\bar{D}$	weighted average of the diffusion coefficients of M_{aq}^{z+} and NP (m^2 s^{-1})
Δ_P	dynamic index for nanoparticulate complexes
$\bar{f}_B$	Boltzmann equilibrium partitioning factor
$\bar{f}_{el,a}$	electrostatic coefficient for conductive diffusion towards the NP
$\bar{f}_{el,d}$	electrostatic coefficient for conductive diffusion away from the NP
J_{dif}^*	diffusion controlled flux from bulk medium to macroscopic surface (mol m^{-2} s^{-1})
J_{kin}	kinetically controlled flux for dissociation of MS within the macroscopic reaction layer (mol m^{-2} s^{-1})
κ_p^{-1}	intraparticulate Debye length (m)
K_{int}	intrinsic stability constant for MS (m^3 mol^{-1})
k_a	overall rate constant for complex formation (m^3 mol^{-1} s^{-1})
$k_{a,p}$	rate constant for diffusive supply of M_{aq}^{z+} to a 3D NP (m^3 mol^{-1} s^{-1})

k_a^{is}	rate constant for inner-sphere complex formation from the precursor outer-sphere complex in a 3D NP (m^3 mol^{-1} s^{-1})
$k_{d,p}$	rate constant for diffusion of M_{aq}^{z+} away from a 3D NP (s^{-1})
k_d^{is}	rate constant for inner-sphere complex dissociation in a 3D NP (s^{-1})
k_w	inner-sphere dehydration rate constant of hydrated metal ions (s^{-1})
$\mathcal{L}_{NP}$	lability index for nanoparticulate MS at a macroscopic reactive interface
λ_{NP}	thickness of the intraparticulate reaction layer for a 3D nanoparticle (m)
$\overline{\lambda}$	thickness of the operational reaction layer at the macroscopic interface (m)
N_S	number of binding sites S per NP
r_0	electrode radius (m)
r_p	particle radius (m)
$R_{a,p}$	rate of diffusive supply of M_{aq}^{z+} towards a 3D NP (mol m^{-3} s^{-1})
R_a^{is}	rate of inner-sphere complex formation in a 3D NP (mol m^{-3} s^{-1})
$R_{d,p}$	rate of diffusive efflux of M_{aq}^{z+} away from a 3D NP (mol m^{-3} s^{-1})
R_d^{is}	rate of inner-sphere complex dissociation in a 3D NP (mol m^{-3} s^{-1})
ϕ^*	volume fraction of an NP in the bulk dispersion
ϕ_λ	volume fraction of an NP that lies within the operational reaction layer at a macroscopic interface
τ_{diff}	characteristic timescale for extraparticulate diffusion (s)
τ_{diss}	characteristic timescale for MS dissociation (s)
V^{os}	volume for an outer-sphere associate between M_{aq}^{z+} and an individual site S (m^3)

References

(1) Commission Recommendation of 18 October 2011 on the definition of nanomaterial. *Official Journal of the European Union*, L 275/38 (2011/696/EU)

(2) van Leeuwen, H. P.; Buffle, J.; Duval, J. F. L.; Town, R. M. Understanding the extraordinary ionic reactivity of aqueous nanoparticles. *Langmuir* **2013**, *29*, 10297-10302.

(3) Town, R. M.; Buffle, J.; Duval, J. F. L.; van Leeuwen, H. P. Chemodynamics of soft charged nanoparticles in aquatic media: fundamental concepts. *J. Phys. Chem. A* **2013**, *117*, 7643-7654.

(4) Polyakov, P. D.; Duval, J. F. L. Speciation dynamics of metals in dispersion of nanoparticles with discrete distribution of charged binding sites. *Phys. Chem. Chem. Phys.* **2014**, *16*, 1999-2010.

(5) Qian, S.; Duval, J. F. L. Metal speciation dynamics in dispersions of soft colloidal ligand particles under steady-state laminar flow condition. *J. Phys. Chem. A* **2009**, *113*, 12791-12804.

(6) Duval, J. F. L.; Busscher, H. J.; van de Belt-Gritter, B.; van der Mei, H. C.; Norde, W. Analysis of the interfacial properties of fibrillated and nonfibrillated oral streptococcal strains from electrophoretic mobility and titration measurements: evidence for the shortcomings of the 'classical soft-particle approach'. *Langmuir* **2005**, *21*, 11268-11282.

(7) Rotureau, E.; Thomas, F.; Duval, J. F. L. Relationship between swelling and the electrohydrodynamic properties of functionalized carboxymethyldextran macromolecules. *Langmuir* **2007**, *23*, 8460-8473.

(8) Duval, J. F. L.; Slaveykova, V. I.; Hosse, M.; Buffle, J.; Wilkinson, K. J. Electrohydrodynamic properties of succinoglycan as probed by fluorescence correlation spectroscopy, potentiometric titration and capillary electrophoresis. *Biomacromolecules* **2006**, *7*, 2818-2826.

(9) Buffle, J.; Zhang, Z.; Startchev, K. Metal flux and dynamic speciation at (bio)interfaces. Part I: Critical evaluation and compilation of physicochemical parameters for complexes with simple ligands and fulvic/humic substances. *Environ. Sci. Technol.* **2007**, *41*, 7609-7620.

(10) Park, D. E.; Lee, S. J.; Lee, J.-H.; Choi, M. Y.; Han, S. W. Effect of polymeric stabilizers on the catalytic activity of Pt nanoparticles synthesized by laser ablation. *Chem. Phys. Lett.* **2010**, *484*, 254−257.

(11) Giret, S.; Man, M. W. C.; Carcel, C. Mesoporous-silica-functionalized nanoparticles for drug delivery. *Chem. Eur. J.* **2015**, *21*, 13850-13865.

(12) Botelho, C. M. S.; Boaventura, R. A. R.; Gonçalves, M. L. S. S. Interactions of Pb(II) with particles of a polluted river *Anal. Chim. Acta.* **2002**, *462*, 73-85.

(13) Botelho, C. M. S.; Boaventura, R. A. R.; Gonçalves, M. L. S. S. Copper complexation with soluble and surface freshwaters ligands. *Electroanalysis* **2002**, *14*, 1713-1721.

(14) Mota, A. M.; Correia dos Santos, M. M. In *Metal Speciation and Bioavailibility*; Tessier A., Turner, D., Eds.; John Wiley and Sons: New York, 1995; Chapter 5.

(15) van Leeuwen, H. P.; Town, R. M.; Buffle, J.; Cleven, R. F. M. J.; Davison, W.; Puy, J.; van Riemsdijk, W. H.; Sigg, L. Dynamic speciation analysis and bioavailability of metals in aquatic systems. *Environ. Sci. Technol*. **2005**, *39*, 8545-8556.

(16) Turner, D. R.; Whitfield, M. The reversible electrodeposition of trace metal ions from multi-ligand systems. Part I. Theory. *J. Electroanal. Chem.* **1979**, *103*, 43-60.

(17) Cleven, R. F. M. J. *Heavy metal/polyacid interaction. An electrochemical study of the binding of Cu(II), Pb(II) and Zn(II) to polycarboxylic and humic acids.* PhD Thesis, Wageningen Agricultural University: The Netherlands, 1984.

(18) Buffle, J.; Tercier-Waeber, M. L. In situ voltammetry: concepts and practice for trace analysis and speciation. In: Buffle, J.; Horvai, G. (eds) *In Situ Monitoring of Aquatic Systems: Chemical Analysis and Speciation*. John Wiley & Sons: Chichester, 2000, pp. 279-405.

(19) Garcés, J. L.; Mas, F.; Cecília, J.; Puy, J.; Galceran, J.; Salvador, J. Voltammetry of heterogeneous labile metal-macromolecular systems for any ligand-to-metal ratio. Part I. Approximate voltammetric expressions for the limiting current to obtain complexation information. *J. Electroanal. Chem.* **2000**, *484*, 107-119.

(20) Alfaro-de la Torre, M. C.; Beaulieu, P. -Y.; Tessier, A. In situ measurement of trace metals in lakewater using the dialysis and DGT techniques. *Anal. Chim. Acta* **2000**, *418*, 53-68.

(21) Davison, W.; Zhang, H. 2012. Progress in understanding the use of diffusive gradients in thin films (DGT) – back to basics. *Environ. Chem*. **9**, 1-13.

(22) Galceran, J.; Puy, J. Interpretation of diffusion gradients in thin films (DGT) measurements: a systematic approach. *Environ. Chem.* **2015**, *12*, 112-122.

(23) Weng, L.; van Riemsdijk, W. H.; Temminghof, E. J. M. Kinetic aspects of Donnan membrane technique for measuring free trace cation concentration. *Anal. Chem.* **2005**, *77*, 2852-2861.

(24) Weng, L.; van Riemsdijk, W. H.; Temminghoff, E. J. M. Effects of lability of metal complex on free ion measurement using DMT. *Environ. Sci. Technol.* **2010**, *44*, 2529-2534.

(25) Buffle, J.; Parthasarathy, N.; Djane, N. -K.; Matthiasson, L. Permeation liquid membranes for field analysis and speciation of trace compounds in natural waters. In: Buffle, J.; Horvai, G. (eds) *In Situ Monitoring of Aquatic Systems: Chemical Analysis and Speciation*. John Wiley & Sons: Chichester, 2000, pp. 407-493.

(26) Tomaszewski, L.; Buffle, J.; Galceran, J. Theoretical and analytical characterization of a flow-through permeation liquid membrane with controlled flux for metal speciation measurements. *Anal. Chem.* **2003**, *75*, 893-900.

(27) Gunkel-Grillon, P.; Buffle, J. Speciation of Cu(II) with a flow-through permeation liquid membrane: discrimination between free copper, labile and inert Cu(II) complexes, under natural water conditions. *Analyst* **2008**, *133*, 954-961.

(28) Viana, M. M. O.; da Silva, M. P.; Agraz, R.; Procopio, J. R.; Sevilla, M. T.; Hernandez, L. Comparison of two kinetic approaches for copper speciation using ion-exchange columns and ion-exchange modified carbon paste electrodes. *Anal. Chim. Acta* **1999**, *382*, 179-188.

(29) Muller, F. L. L.; Kester, D. R. Kinetic approach to trace metal complexation in seawater: application to zinc and cadmium. *Environ. Sci. Technol.* **1990**, *24*, 234-242.

(30) Procopio, J. R.; Viana, M. D. M. O.; Hernandez, L. H. Microcolumn ion-exchange method for kinetic speciation of copper and lead in natural waters. *Environ. Sci. Technol.* **1997**, *31*, 3081-3085.

(31) Haftka, J. J. H.; Parsons, J. R.; Govers, H. A. J.; Ortega-Calvo, J. -J. Enhanced kinetics of solid-phase microextraction and biodegradation of polycyclic aromatic hydrocarbons in the presence of dissolved organic matter. *Environ. Toxicol. Chem.* **2008**, *27*, 1526-1532.

(32) ter Laak, T. L.; ter Bekke, M. A.; Hermens, J. L. M. Dissolved organic matter enhances transport of PAHs to aquatic organisms. *Environ. Sci. Technol.* **2009**, *43*, 7212-7217.

(33) Bayen, S.; ter Laak, T. L.; Buffle, J.; Hermens, J. L. M. Dynamic exposure of organisms and passive samplers to hydrophobic chemicals. *Environ. Sci. Technol.* **2009**, *43*, 2206-2215.

(34) Zielińska, K.; van Leeuwen, H. P.; Thibault, S.; Town, R. M. Speciation analysis of aqueous nanoparticulate diclofenac complexes by solid-phase microextraction. *Langmuir* **2012**, *28*, 14672-14680.

(35) Buffle, J. *Complexation Reactions in Aquatic Systems: an Analytical Approach.* Ellis Horwood: Chichester, 1988.

(36) Koutecký, J.; Koryta, J. The general theory of polarographic kinetic currents. *Electrochim. Acta* **1961**, *3*, 318-339.

(37) Heyrovský, J.; Kůta, J. *Principles of Polarography*. Academic Press: New York, 1966.

(38) Koryta, J,; Dvorak, J.; Kavan, L. *Principles of Electrochemistry*, 2nd edn. Wiley: Chichester, 1993.

(39) van Leeuwen, H. P.; Puy, J.; Galceran, J.; Cecília, J. Evaluation of the Koutecký-Koryta approximation for voltammetric currents generated by metal complex systems with various labilities. *J. Electroanal. Chem.* **2002**, *526*, 10-18.

(40) van Leeuwen, H. P.; Town, R. M. Stripping chronopotentiometry at scanned deposition potential (SSCP). Part 7. Kinetic currents for ML_2 complexes. *J. Electroanal. Chem.* **2006**, *587*, 148-154.

(41) Buffle, J.; Startchev, K.; Galceran, J. Computing steady-state metal flux at microorganism and bioanalogical sensor interfaces in multiligand systems. A reaction layer approximation and its comparison with the rigorous solution. *Phys. Chem. Chem. Phys*. **2007**, *9*, 2844-2855.

(42) van Leeuwen, H. P.; Town, R. M. Protonation effects on dynamic flux properties of aqueous metal complexes. *Collect. Czech. Chem. Commun*. **2009**, *74*, 1543-1557.

(43) van Leeuwen, H. P.; Town, R. M. Lability of nanoparticulate metal complexes in electrochemical speciation analysis. *J. Solid State Electrochem.* **2016**, in press, DOI 10.1007/s10008-016-3372-7.

(44) Pinheiro, J. P.; Minor, M.; van Leeuwen, H. P. Metal speciation dynamics in colloidal ligand dispersions. *Langmuir* **2005**, *21*, 8635-8642.

(45) Ohshima, H.; Kondo, T. Relationship among the surface potential, Donnan potential and charge density of ion-penetrable membranes. *Biophys. Chem.* **1990**, *38*, 117-122.

(46) Duval, J. F. L. Electrokinetics of soft interfaces. 2. Analysis based on the nonlinear Poisson-Boltzmann equation. *Langmuir* **2005**, *21*, 3247-3258.

(47) van Leeuwen, H. P. Eigen kinetics in surface complexation of aqueous metal ions. *Langmuir* **2008**, *24*, 11718-11721.

(48) Eigen M. Fast elementary steps in chemical reaction mechanisms. *Pure Appl. Chem*. **1963**, *6*, 97-116.

(49) Crank, J. *The Mathematics of Diffusion*. Oxford Science Publications: Oxford, 1979.

(50) van Leeuwen, H. P.; Buffle, J. Chemodynamics of aquatic metal complexes: from small ligands to colloids. *Environ. Sci. Technol.* **2009**, *43*, 7175-7183.

(51) Duval, J. F. L.; van Leeuwen, H. P. Rates of ionic reactions with charged nanoparticles in aqueous media. *J. Phys. Chem. A* **2012**, *116*, 6443-6451.

(52) Zhang, Z.; Buffle, J.; van Leeuwen, H. P. Roles of dynamic metal speciation and membrane permeability in metal flux through lipophilic membranes: general theory and experimental validation with nonlabile complexes. *Langmuir* **2007**, *23*, 5216-5226.

(53) Morel, F. M. M.; Hering, J. G. *Principles and Applications of Aquatic Chemistry*. Wiley-Interscience: New York, 1993.

(54) Sokol, L. S. W. L.; Fink, T. D.; Rorabacher, D. B. Kinetics of inner-sphere solvent exchange on the aquocopper(II) ion: indirect determination from kinetics of copper(II) reacting with ammonia in aqueous solution. *Inorg. Chem*. **1980**, *19*, 1263−1266.

(55) Powell, D. H.; Helm, K.; Merbach, A. E. ^{17}O nuclear magnetic resonance in aqueous solutions of Cu^{2+}: the combined effect of Jahn-Teller inversion and solvent exchange on relaxation rates. *J. Chem. Phys.* **1991**, *95*, 9258−9265.

(56) Kobayashi, S.; Nagayama, S.; Busujima, T. Lewis acid catalysts stable in water. Correlation between catalytic activity in water and hydrolysis constants and exchange rate constants for substitution of inner-sphere water ligands. *J. Am. Chem. Soc.* **1998**, *120*, 8287-8288.

(57) Swift, T. J.; Connick, R. E. NMR-relaxation mechanisms of O^{17} in aqueous solutions of paramagnetic cations and the lifetime of water molecules in the first coordination sphere. *J. Chem. Phys.* **1962**, *37*, 307−320.

(58) Connick, R. E.; Fiat, D. Oxygen-17 nuclear magnetic resonance study of the hydration shell of nickelous ion. *J. Chem. Phys.* **1966**, *44*, 4103−4107.

(59) Gazzaz, H. A.; Ember, E.; Zahl, A.; van Eldik, R. Mechanistic information from volume profiles for water exchange and complex formation reactions of aquated Ni(II). pH, buffer and medium effects. *Dalton Trans*. **2009**, 9486−9495.

(60) Levich, V. G. *Physicochemical Hydrodynamics*. Prentice-Hall: Englewood Cliffs, NJ, 1962.

(61) Xie, H. A geometrical model for coalescing aerosol particles. *J. Aerosol Sci.* **2008**, *39*, 277-285.

(62) Town, R. M.; van Leeuwen, H. P. Intraparticulate speciation analysis of soft nanoparticulate metal complexes. The impact of electric condensation on the binding of Cd^{2+}/Pb^{2+}/Cu^{2+} by humic acids. *Phys. Chem. Chem. Phys.* **2016**, *18*, 10049-10058.

(63) Huang, Q. R.; Dubin, P. L.; Moorefield, C. N.; Newkome, G. R. Counterion binding on charged spheres: effect of pH and ionic strength on the mobility of carboxyl-terminated dendrimers. *J. Phys. Chem. B.* **2000**, *104*, 898-904.

(64) Li, Z.; van Dyk, A. K.; Fitzwater, S. J.; Fichthorn, K. A.; Milner, S. T. Atomistic molecular dynamics simulations of charged latex particle surfaces in aqueous solution. *Langmuir* **2016**, *32*, 428-441.

(65) von Stackelberg, M. O.; Pilgram, M.; Toome, V. Bestimmung von Diffusionskoeffizienten einiger Ionen in wäβriger Lösung in Gegenwart von Fremdelektrolyten. I. *Z. Elektrochem.* **1953**, *57*, 342−350.

(66) Einstein, A. Über die von der molekularkinetischen Theorie der Wärme geforderte Bewegung von in ruhenden Flüssigkeiten suspendierten Teilchen. *Annal. Phys*. **1905**, *322*, 549−560.

(67) Zhang, H.; Davison, W. Performance characteristics of diffusion gradients in thin films for the in situ measurement of trace metals in aqueous solution. *Anal. Chem.* **1995**, *67*, 3391-3400.

(68) Galceran, J.; Puy, J.; Salvador, J.; Cecilía, J.; van Leeuwen, H. P. Voltammetric lability of metal complexes at spherical microelectrodes with various radii. *J. Electroanal. Chem.* **2001**, *505*, 85-94.

(69) Pinheiro, J. P.; van Leeuwen, H. P. Metal speciation dynamics and bioavailability. 2. Radial diffusion effects in the microorganism range. *Environ. Sci. Technol.* **2001**, *35*, 894-900.

(70) van Leeuwen, H. P.; Town, R. M. Stripping chronopotentiometry for metal ion speciation analysis at a microelectrode. *J. Electroanal. Chem.* **2002**, *523*, 16-25.

(71) Tsekov, R.; Kovač, S.; Žutić, V. Attachment of oil droplets and cells on dropping mercury electrode. *Langmuir* **1999**, *15*, 5649-5653

(72) Ivošević DeNardis, N.; Žutić, V.; Svetličić, V.; Frkanec, R. Amperometric adhesion signals of liposomes, cells and droplets. *Chem. Biochem. Eng. Q.* **2009**, *23*, 87-92.

Table of Contents Graphic